Appl. Math. Mech. -Engl. Ed., **41**(5), 805–818 (2020)

Applied Mathematics and Mechanics (English Edition)

https://doi.org/10.1007/s10483-020-2606-5

A hybrid multi-degree-of-freedom vibration isolation platform for spacecrafts by the linear active disturbance rejection control*

Weichao CHI[1,2,†], S. J. MA[3], J. Q. SUN[3]

1. College of Science, Northeastern University, Shenyang 100819, China;
2. Key Laboratory of Ministry of Education on Safe Mining of Deep Metal Mines, Northeastern University, Shenyang 100819, China;
3. Department of Mechanical Engineering, School of Engineering, University of California, Merced, CA 95343, U. S. A.

(Received Oct. 31, 2019 / Revised Feb. 19, 2020)

Abstract The hybrid vibration isolation, which takes advantages of both the passive and active approaches, has been an important solution for space missions. The objective of this paper is to design a vibration isolation platform for payloads on spacecrafts with the robust, wide bandwidth, and multi-degree-of-freedom (MDOF). The proposed solution is based on a parallel mechanism with six voice-coil motors (VCMs) as the actuators. The linear active disturbance resistance control (LADRC) algorithm is used for the active control. Numerical simulation results show that the vibration isolation platform performs effectively over a wide bandwidth, and the resonance introduced by the passive isolation is eliminated. The system robustness to the uncertainties of the structure is also verified by simulation.

Key words hybrid vibration isolation, Stewart platform, linear active disturbance rejection control (LADRC), stability, robustness

Chinese Library Classification O328
2010 Mathematics Subject Classification 70Q05

1 Introduction

During the orbital missions of spacecrafts, the vibration caused by several sources, such as reaction wheels (RWs), control moment gyroscopes (CMGs), solar array drives, and cryocoolers, is always a serious negative impact on the precision payloads. In order to reduce the vibration transmission from the vibration sources to the payloads, one of the most intuitive methods is to introduce a vibration isolation device in the transmission path to isolate the static instrument from the vibrating structure.

* Citation: CHI, W. C., MA, S. J., and SUN, J. Q. A hybrid multi-degree-of-freedom vibration isolation platform for spacecrafts by the linear active disturbance rejection control. *Applied Mathematics and Mechanics* (*English Edition*), **41**(5), 805–818 (2020) https://doi.org/10.1007/s10483-020-2606-5

† Corresponding author, E-mail: chiweichao@gmail.com

Project supported by the National Natural Science Foundation of China (No. 11572215), the Fundamental Research Funds for the Central Universities (No. N160503002), and the China Scholarship Council

The design of the vibration isolation structure depends on the type and the frequency of the disturbance. As the frequency range of vibration sources covers from low frequency to high frequency, a wide bandwidth of the vibration isolator is demanded. The commonly used passive vibration isolation methods that consist of mass-spring-damper systems work well on high frequency attenuation, but the performance on low frequency is usually limited by the stiffness of the structure, and the additional resonance at some specific frequencies is also a serious defect. The hybrid isolation that combines passive and active methods was introduced to overcome the defects in passive damping. The active part of the hybrid isolation system can provide real-time force according to the sensor's feedback under certain control law. In the past decade, the hybrid vibration isolation has become a practical approach and has been widely used for the improving performance of microprocessors, actuators, and sensors. Cobb et al.[1] presented a hybrid isolation strut using least mean squares (LMS) control to suppress the vibration in certain broadband. Zhou and Li[2] designed an intelligent vibration isolation platform with piezoelectric actuators bonded to the beams. Zhang et al.[3] presented a novel active-passive hybrid vibration control for truss enveloping CMGs on satellites.

The isolation structure is the basis of a hybrid vibration isolation system. It supports or connects the payload to the main body, and meanwhile, plays the role of passive vibration isolation. Many forms of structures have been studied in order to isolate vibration in multiple-degree-of-freedom (MDOF), in which the Stewart platform is one of the best performing structures for its 6 degrees of freedom (6-DOF) attitude maneuvering ability[4]. The platform was invented for flight simulating, soon applied to mechanical machining, precision positioning, vibration isolation, and many other fields[5]. A Stewart platform consists of six extensible legs with universal joints or spherical joints at each end, connecting the payload-platform to the base-platform, as shown in Fig. 1. Fichter[6] and Bonev and Ryu[7] solved the kinematics problem of a general Stewart platform. Lebert et al.[8] presented the dynamic model of Stewart platform using the Lagrange method. Xu and Wang[9] developed a closed-form dynamic model of a Stewart platform with proportional-derivative (PD) control. Wu et al.[10] proposed a new decoupling condition of stiffness matrix based on the elegant algebraic approach to express the dynamic isotropy index of natural frequencies.

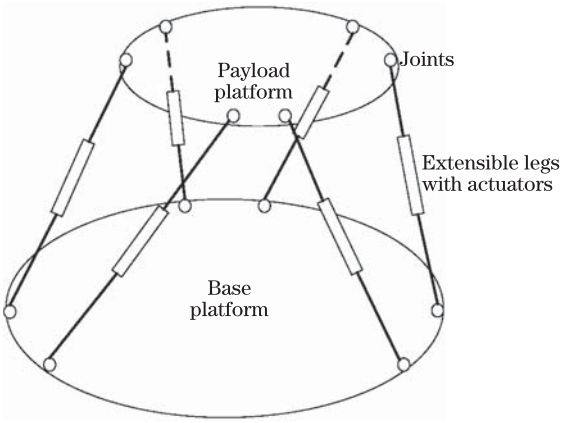

Fig. 1 A general Stewart platform

On the other hand, the controller design is the key issue for the active part of a hybrid vibration isolation system. The control algorithm is used to determine the actuator input by designing the transfer relationship between the system input and feedback signals. Gáspár et al.[11] and Zhang et al.[12] analyzed the various uncertainties in vibration isolation structures and the corresponding mathematical descriptions, and designed a robust control system for vibration isolation based on the analysis of uncertainties. At the same time, a great number of

recent studies aim at the controlling for systems with uncertainties and inaccurate mathematical model, by using nonlinear control and intelligent control algorithms. The active disturbance rejection control (ADRC)[13], fuzzy active control[14], artificial neural network control[15], and genetic algorithm[16] were studied to resolve the difficulties of modeling complex systems and nonlinearities. Gao[17] gave a method to determine the observer and controller parameters of linear active disturbance rejection control (LADRC) by the concept of bandwidth. That made the controller parameters easy to tune, and the physical meaning of the parameters is clearer in practical vibration engineering.

In this paper, a practical approach for designing a hybrid MDOF vibration isolation platform is proposed. The contributions of this paper are listed as follows:

(i) We extend the LADRC method to the hybrid vibration isolation problem of space parallel structures for the first time, leading to a controller that can reject the disturbances due to external excitations and dynamic couplings of the system.

(ii) We also report extensive results of the effect of control parameters on vibration isolation bandwidth, present the proof of stability, and study the robustness of the control with respect to the modeling error.

The paper is organized as follows. In the second section, the dynamical model of the Stewart platform is established with the Newton-Euler method in the task space. In the third section, an LADRC control strategy is presented for the control of multi-input multi-output (MIMO) system with parameter uncertainty and external disturbance. In the fourth section, the effectiveness of the approach is verified by numerical simulation.

2 Design and modeling of the vibration isolation structure

2.1 System configuration and reference frames definitions

The Stewart platform presented in this paper is a general form with six extensible legs connecting the base-platform and the payload-platform. Each leg is equipped with a voice coil motor (VCM) as the actuator. The stator and the mover of the VCM are connected by a piece of diaphragm spring, and the movement is also constrained by a linear bearing to ensure that the voice coil moves along the axle. The stator and the mover are respectively treated as the lower and the upper legs together with the other components, such as struts, then the lower and the upper legs are connected to the base-platform and the payload-platform by spherical joints at each end, respectively.

Define the coordinate frames B and P, which are attached to the base and the payload platforms, respectively, and the origins are the mass centers of the base- and payload-platforms, respectively. The coordinate frames D and U are attached to the lower and upper legs, respectively. The relationship between the inertial frame O and the local frames B, P, D, and U is shown in Fig. 2.

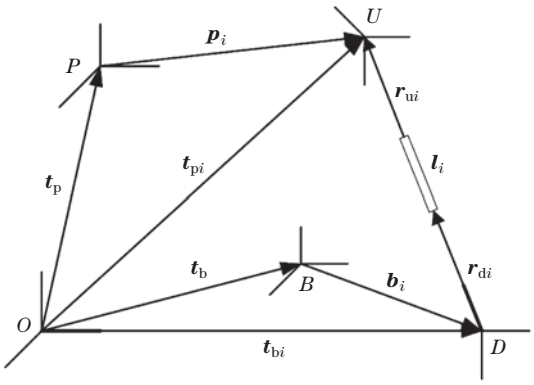

Fig. 2 Relationship between inertial and local frames

2.2 Dynamic analysis of the payload

The position vectors of upper and lower ends of the ith leg in the inertial frame O can be derived from the position vectors of frames P and B as

$$\begin{cases} \boldsymbol{t}_{\mathrm{p}i} = \boldsymbol{t}_{\mathrm{p}} + \boldsymbol{p}_i, \\ \boldsymbol{t}_{\mathrm{b}i} = \boldsymbol{t}_{\mathrm{b}} + \boldsymbol{b}_i. \end{cases} \tag{1}$$

From the subtraction of $\boldsymbol{t}_{\mathrm{p}i}$ and $\boldsymbol{t}_{\mathrm{b}i}$, we can get the vector of the ith leg as

$$\boldsymbol{l}_i = \boldsymbol{t}_{\mathrm{p}i} - \boldsymbol{t}_{\mathrm{b}i} = (\boldsymbol{t}_{\mathrm{p}} + \boldsymbol{p}_i) - (\boldsymbol{t}_{\mathrm{b}} + \boldsymbol{b}_i). \tag{2}$$

The velocities of upper and lower ends of the leg can be expressed as

$$\begin{cases} \dot{\boldsymbol{t}}_{\mathrm{p}i} = \dot{\boldsymbol{t}}_{\mathrm{p}} + \boldsymbol{\omega}_{\mathrm{p}} \times \boldsymbol{p}_i, \\ \dot{\boldsymbol{t}}_{\mathrm{b}i} = \dot{\boldsymbol{t}}_{\mathrm{b}} + \boldsymbol{\omega}_{\mathrm{b}} \times \boldsymbol{b}_i, \end{cases} \tag{3}$$

where $\boldsymbol{\omega}_{\mathrm{p}}$ and $\boldsymbol{\omega}_{\mathrm{b}}$ are the angular velocity vectors of the payload and the base, respectively. Then, the velocity of the ith leg is

$$\begin{aligned} \dot{l}_i &= (\dot{\boldsymbol{t}}_{\mathrm{p}i} - \dot{\boldsymbol{t}}_{\mathrm{b}i}) \cdot \boldsymbol{\tau}_i = (\dot{\boldsymbol{t}}_{\mathrm{p}} + (\boldsymbol{\omega}_{\mathrm{p}} \times \boldsymbol{p}_i) - \dot{\boldsymbol{t}}_{\mathrm{b}} + \boldsymbol{\omega}_{\mathrm{b}} \times \boldsymbol{b}_i) \cdot \boldsymbol{\tau}_i \\ &= \begin{pmatrix} \boldsymbol{\tau}_i^{\mathrm{T}} & (\boldsymbol{p}_i \times \boldsymbol{\tau}_i)^{\mathrm{T}} \end{pmatrix} \begin{pmatrix} \dot{\boldsymbol{t}}_{\mathrm{p}} \\ \boldsymbol{\omega}_{\mathrm{p}} \end{pmatrix} - \begin{pmatrix} \boldsymbol{\tau}_i^{\mathrm{T}} & (\boldsymbol{b}_i \times \boldsymbol{\tau}_i)^{\mathrm{T}} \end{pmatrix} \begin{pmatrix} \dot{\boldsymbol{t}}_{\mathrm{b}} \\ \boldsymbol{\omega}_{\mathrm{b}} \end{pmatrix}, \end{aligned} \tag{4}$$

where $\boldsymbol{\tau}_i = \boldsymbol{l}_i / l_i$ is the unit vector along the leg. To simplify the matrix form of the length vector, let

$$\begin{aligned} \boldsymbol{H}_{\mathrm{p}} &= \begin{pmatrix} \boldsymbol{\tau}_1 & \cdots & \boldsymbol{\tau}_6 \\ \boldsymbol{p}_1 \times \boldsymbol{\tau}_1 & \cdots & \boldsymbol{p}_6 \times \boldsymbol{\tau}_6 \end{pmatrix}, \\ \boldsymbol{H}_{\mathrm{b}} &= \begin{pmatrix} \boldsymbol{\tau}_1 & \cdots & \boldsymbol{\tau}_6 \\ \boldsymbol{b}_1 \times \boldsymbol{\tau}_1 & \cdots & \boldsymbol{b}_6 \times \boldsymbol{\tau}_6 \end{pmatrix}, \\ \boldsymbol{x}_{\mathrm{p}} &= \begin{pmatrix} \boldsymbol{t}_{\mathrm{p}} \\ \boldsymbol{\theta}_{\mathrm{p}} \end{pmatrix}, \quad \boldsymbol{x}_{\mathrm{b}} = \begin{pmatrix} \boldsymbol{t}_{\mathrm{b}} \\ \boldsymbol{\theta}_{\mathrm{b}} \end{pmatrix}. \end{aligned}$$

Equation (4) can be written as

$$\dot{\boldsymbol{l}} = \boldsymbol{H}_{\mathrm{p}}^{\mathrm{T}} \dot{\boldsymbol{x}}_{\mathrm{p}} - \boldsymbol{H}_{\mathrm{b}}^{\mathrm{T}} \dot{\boldsymbol{x}}_{\mathrm{b}}. \tag{5}$$

The force between the upper and lower legs is

$$\boldsymbol{F} = -\boldsymbol{K}(\boldsymbol{l} - \boldsymbol{l}_0) - \boldsymbol{C}\dot{\boldsymbol{l}} + \boldsymbol{F}_1, \tag{6}$$

where $\boldsymbol{F} = (F_1, \cdots, F_6)^{\mathrm{T}}$, $\boldsymbol{l} = (l_1, \cdots, l_6)^{\mathrm{T}}$, $\boldsymbol{F}_1 = (F_{11}, \cdots, F_{16})^{\mathrm{T}}$ is the force vector of the VCMs, and $\boldsymbol{K} = \mathrm{diag}(k_1, \cdots, k_6)$ and $\boldsymbol{C} = \mathrm{diag}(c_1, \cdots, c_6)$ are the stiffness and damping matrices of the legs, respectively.

From Eqs. (5) and (6), the force vector $\boldsymbol{F}$ can be expressed as

$$\boldsymbol{F} = -\boldsymbol{K}\left(\boldsymbol{H}_{\mathrm{p}}^{\mathrm{T}} \dot{\boldsymbol{x}}_{\mathrm{p}} - \boldsymbol{H}_{\mathrm{b}}^{\mathrm{T}} \dot{\boldsymbol{x}}_{\mathrm{b}}\right) - \boldsymbol{C}\boldsymbol{H}_{\mathrm{p}}^{\mathrm{T}} \dot{\boldsymbol{x}}_{\mathrm{p}} + \boldsymbol{C}\boldsymbol{H}_{\mathrm{b}}^{\mathrm{T}} \dot{\boldsymbol{x}}_{\mathrm{b}} + \boldsymbol{F}_1. \tag{7}$$

The free body diagram of the payload platform is shown in Fig. 3. M_{p} is the total mass, $\boldsymbol{F}_{\mathrm{w}}$ and $\boldsymbol{M}_{\mathrm{w}}$ are the external force and torque, respectively, and $\boldsymbol{r}$ and $\boldsymbol{r}_0$ are the position vectors of the mass center of the payload platform in inertial frame and local frame, respectively. The position vector of the mass center is

$$\boldsymbol{r} = \boldsymbol{R}_{\mathrm{p}} \boldsymbol{r}_0. \tag{8}$$

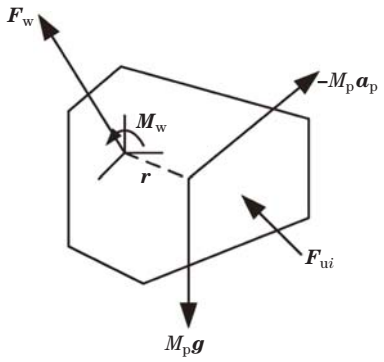

Fig. 3 The force analysis of the top platform

According to Newton's dynamical law, the dynamic equation of the payload platform is

$$M_{\mathrm{p}}\boldsymbol{g} + \boldsymbol{F}_{\mathrm{w}} + \sum_{i=1}^{6} \boldsymbol{F}_{\mathrm{u}i} = M_{\mathrm{p}}\boldsymbol{a}_{\mathrm{p}}, \tag{9}$$

where $\boldsymbol{g}$ is the gravitational acceleration, and $\boldsymbol{a}_{\mathrm{p}}$ is the mass center acceleration defined as

$$\boldsymbol{a}_{\mathrm{p}} = \ddot{\boldsymbol{t}}_{\mathrm{p}} + \boldsymbol{\alpha}_{\mathrm{p}} \times \boldsymbol{r} + \boldsymbol{\omega}_{\mathrm{p}} \times (\boldsymbol{\omega}_{\mathrm{p}} \times \boldsymbol{r}), \tag{10}$$

where $\boldsymbol{\alpha}_{\mathrm{p}}$ and $\boldsymbol{\omega}_{\mathrm{p}}$ are the angular acceleration and the angular velocity, respectively. The balance equation of the control force and inertia force on the payload platform according to the Euler equation is

$$-\sum_{i=1}^{6} \boldsymbol{p}_i \times \boldsymbol{F}_{\mathrm{u}i} + \sum_{i=1}^{6} \boldsymbol{f}_i + \boldsymbol{M}_{\mathrm{w}} + M_{\mathrm{p}}\boldsymbol{r} \times \boldsymbol{g} = \boldsymbol{I}_{\mathrm{p}}^{*}\boldsymbol{\alpha}_{\mathrm{p}} + \boldsymbol{\omega}_{\mathrm{p}} \times \boldsymbol{I}_{\mathrm{p}}^{*}\boldsymbol{\omega}_{\mathrm{p}}, \tag{11}$$

where $\boldsymbol{f}_i$ is the force of the legs, $\boldsymbol{M}_{\mathrm{w}}$ is the sum of external moments, and $\boldsymbol{I}_{\mathrm{p}}^{*}$ is the moment of translating $\boldsymbol{I}_{\mathrm{p}}$ to centroid which can be expressed as

$$\boldsymbol{I}_{\mathrm{p}}^{*} = \boldsymbol{I}_{\mathrm{p}} + M_{\mathrm{p}}(\boldsymbol{r}^{\mathrm{T}}\boldsymbol{r}\boldsymbol{E}_3 - \boldsymbol{r}\boldsymbol{r}^{\mathrm{T}}), \tag{12}$$

in which $\boldsymbol{E}_3$ is a unit matrix. Equations (6), (9), and (11) can be combined into the dynamical equation of system in the task-space as

$$\boldsymbol{J}_{\mathrm{p}}\ddot{\boldsymbol{x}}_{\mathrm{p}} = \boldsymbol{J}_{\mathrm{b}}\boldsymbol{x}_{\mathrm{b}} + \boldsymbol{H}_{\mathrm{p}}\boldsymbol{F} - \boldsymbol{G} + \boldsymbol{D}, \tag{13}$$

where

$$\begin{cases} \boldsymbol{J}_{\mathrm{p}} = \begin{pmatrix} M_{\mathrm{p}}\boldsymbol{E}_3 & -M_{\mathrm{p}}\widetilde{\boldsymbol{r}} \\ 0 & \boldsymbol{I}_{\mathrm{p}}^* \end{pmatrix} + \sum_{i=1}^{6} \begin{pmatrix} \boldsymbol{Q}_{\mathrm{p}i} & -\boldsymbol{Q}_{\mathrm{p}i}\widetilde{\boldsymbol{p}}_i \\ -\widetilde{\boldsymbol{p}}_i\boldsymbol{Q}_{\mathrm{p}i} & \widetilde{\boldsymbol{p}}_i\boldsymbol{Q}_{\mathrm{p}i}\widetilde{\boldsymbol{p}} \end{pmatrix}, \\ \boldsymbol{J}_{\mathrm{b}} = \sum_{i=1}^{6} \begin{pmatrix} \boldsymbol{Q}_{\mathrm{p}i} & -\boldsymbol{Q}_{\mathrm{p}i}\widetilde{\boldsymbol{p}}_i \\ -\widetilde{\boldsymbol{p}}_i\boldsymbol{Q}_{\mathrm{p}i} & \widetilde{\boldsymbol{p}}_i\boldsymbol{Q}_{\mathrm{p}i}\widetilde{\boldsymbol{p}} \end{pmatrix}, \\ \boldsymbol{G} = \begin{pmatrix} -\eta \\ \boldsymbol{\omega}_{\mathrm{p}} \times \boldsymbol{I}_{\mathrm{p}}^*\boldsymbol{\omega}_{\mathrm{p}} - \sum_{i=1}^{6} \boldsymbol{f}_i + \sum_{i=1}^{6} \widetilde{\boldsymbol{p}}_i\boldsymbol{\eta}_{6i} \end{pmatrix}, \\ \boldsymbol{D} = \begin{pmatrix} \boldsymbol{F}_{\mathrm{ext}} \\ \boldsymbol{M}_{\mathrm{ext}} \end{pmatrix} = \begin{pmatrix} \boldsymbol{F}_{\mathrm{w}} + M_{\mathrm{p}}\boldsymbol{g} \\ -\boldsymbol{M}_{\mathrm{w}} - M_{\mathrm{p}}\boldsymbol{r} \times \boldsymbol{g} \end{pmatrix}, \\ \boldsymbol{Q}_{\mathrm{p}i} = m_{\mathrm{u}i}\boldsymbol{\tau}_i\boldsymbol{\tau}_i^{\mathrm{T}} + \dfrac{(\boldsymbol{E}_3 - \boldsymbol{\tau}_i\boldsymbol{\tau}_i^{\mathrm{T}})}{\lambda_i l_i}(m_{\mathrm{u}i}\kappa_i(l_i - l_{\mathrm{u}i}) + m_{\mathrm{d}i}l_{\mathrm{d}i}^2) - \dfrac{1}{\lambda_i l_i}\widetilde{\boldsymbol{\tau}}_i(\boldsymbol{I}_{\mathrm{d}i} + \boldsymbol{I}_{\mathrm{u}i})\widetilde{\boldsymbol{\tau}}_i, \\ \boldsymbol{Q}_{\mathrm{b}i} = \dfrac{(\boldsymbol{E}_3 - \boldsymbol{\tau}_i\boldsymbol{\tau}_i^{\mathrm{T}})}{\lambda_i l_i}(m_{\mathrm{d}i}l_{\mathrm{d}i} + m_{\mathrm{u}i}\kappa_i l_{\mathrm{u}i}) - \dfrac{1}{\lambda_i l_i}\widetilde{\boldsymbol{\tau}}_i(\boldsymbol{I}_{\mathrm{d}i} + \boldsymbol{I}_{\mathrm{u}i})\widetilde{\boldsymbol{\tau}}_i, \\ \lambda_i = 2l_{\mathrm{u}i} + 2l_{\mathrm{d}i} - l_i, \end{cases}$$

in which $m_{\mathrm{u}i}$ and $m_{\mathrm{d}i}$, and $I_{\mathrm{u}i}$ and $I_{\mathrm{d}i}$ are the masses and inertias of the upper and lower legs, respectively. $\boldsymbol{F}_{\mathrm{ext}}$ and $\boldsymbol{M}_{\mathrm{ext}}$ are the external force and moment matrices, respectively, and the calculating sign "˜" denotes the transformation of the column vector $\boldsymbol{x} = (x_1, x_2, x_3)^{\mathrm{T}}$ into

$$\widetilde{\boldsymbol{x}} = \begin{pmatrix} 0 & -x_3 & x_2 \\ x_3 & 0 & -x_1 \\ -x_2 & x_1 & 0 \end{pmatrix}. \tag{14}$$

We can obtain the dynamical equation in the task-space by substituting Eq. (7) into Eq. (13) as

$$\begin{aligned} &\boldsymbol{J}_{\mathrm{p}}\ddot{\boldsymbol{x}}_{\mathrm{p}} + \boldsymbol{H}_{\mathrm{p}}\boldsymbol{C}\boldsymbol{H}_{\mathrm{p}}^{\mathrm{T}}\dot{\boldsymbol{x}}_{\mathrm{p}} + \boldsymbol{H}_{\mathrm{p}}\boldsymbol{K}\boldsymbol{H}_{\mathrm{p}}^{\mathrm{T}}\delta\boldsymbol{x}_{\mathrm{p}} \\ &= \boldsymbol{J}_{\mathrm{b}}\ddot{\boldsymbol{x}}_{\mathrm{b}} + \boldsymbol{H}_{\mathrm{p}}\boldsymbol{K}\boldsymbol{H}_{\mathrm{b}}^{\mathrm{T}}\delta\boldsymbol{x}_{\mathrm{b}} + \boldsymbol{H}_{\mathrm{p}}\boldsymbol{C}\boldsymbol{H}_{\mathrm{b}}^{\mathrm{T}}\dot{\boldsymbol{x}}_{\mathrm{b}} + \boldsymbol{H}_{\mathrm{p}}\boldsymbol{F}_1 - \boldsymbol{G} + \boldsymbol{D}. \end{aligned} \tag{15}$$

As shown in Eq. (15), the payload platform is a second-order plant which is mainly determined by the force from the legs, while it is disturbed by the motion of the base-platform and the external disturbing force.

3 LADRC design for MIMO system

3.1 The LADRC algorithm

LADRC is the linear form of the ADRC. LADRC augments the states with generalized disturbance, and uses the generalized disturbance estimation and the linear feedback to reject the disturbance. It employs the linear extended state observer (LESO) to estimate the dynamic characteristics and the generalized disturbance of the system, and then uses the linear combination of the state errors and the generalized disturbance to determine the final control signal. The diagram of LADRC is shown in Fig. 4.

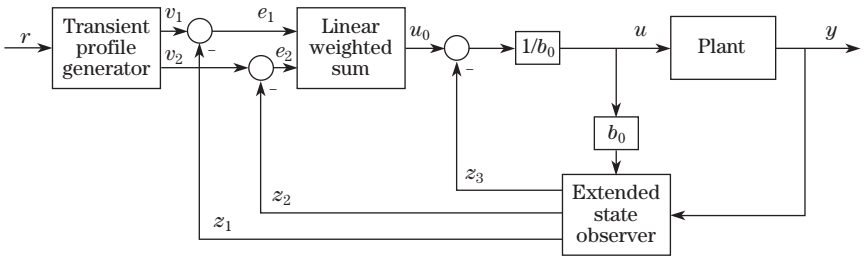

Fig. 4 The diagram of LADRC

To design a control system for the second-order system (15), we consider a general second-order single-input single-output (SISO) system given by

$$\ddot{y} + a_1\dot{y} + a_2 y = b_1\ddot{w} + b_2\dot{w} + b_3 w + bu, \tag{16}$$

where y, u, and w are the output, input, and external disturbances of the plant, respectively. The system parameters a_1, a_2, b_1, b_2, b_3, and b are all unknown.

Equation (16) can be written as

$$\ddot{y} = -a_1\dot{y} - a_2 y + b_1\ddot{w} + b_2\dot{w} + b_3 w + (b - b_0)u + b_0 u = f + b_0 u, \tag{17}$$

where $f = -a_1\dot{y} - a_2 y + b_1\ddot{w} + b_2\dot{w} + b_3 w + (b - b_0)u$ denoted as the generalized disturbance is the key point of the LADRC solution. The internal disturbance $f_1 = -a_1\dot{y} - a_2 y + (b - b_0)u$ and the external disturbance $f_2 = b_1\ddot{w} + b_2\dot{w} + b_3 w$ are together presented in f, which is treated as a new augmented state $x_3 = f$. We then rewrite Eq. (17) as

$$\begin{cases} \dot{x}_1 = x_2, \\ \dot{x}_2 = x_3 + b_0 u, \\ \dot{x}_3 = h, \\ y = x_1, \end{cases} \tag{18}$$

where $x_1 = y$, $x_2 = \dot{x}_1$, $h = \dot{f}$, x_3 is the extended state to be estimated by the observer, and b_0 is an approximate estimate of b in Eq. (16). The state space description of the system is

$$\begin{cases} \dot{\boldsymbol{x}} = \boldsymbol{A}\boldsymbol{x} + \boldsymbol{B}u + \boldsymbol{E}h, \\ y = \boldsymbol{C}x, \end{cases} \tag{19}$$

where

$$\boldsymbol{A} = \begin{pmatrix} 0 & 1 & 0 \\ 0 & 0 & 1 \\ 0 & 0 & 0 \end{pmatrix}, \quad \boldsymbol{B} = \begin{pmatrix} 0 \\ b_0 \\ 0 \end{pmatrix}, \quad \boldsymbol{C} = \begin{pmatrix} 1, 0, 0 \end{pmatrix}, \quad \boldsymbol{E} = \begin{pmatrix} 0 \\ 0 \\ 1 \end{pmatrix}. \tag{20}$$

To estimate the states and the generalized disturbance, we use an observer as

$$\begin{cases} \dot{z}_1 = z_2 + \beta_1 e, \\ \dot{z}_2 = z_3 + \beta_2 e, \\ \dot{z}_3 = \beta_3 e, \end{cases} \tag{21}$$

where z_1, z_2, and z_3 are estimated values of y, $\dot{y}$, and f, respectively. The observer gains β_1, β_2, and β_3 must be chosen to properly place the eigenvalues of $(\boldsymbol{A} - \boldsymbol{L}\boldsymbol{C})$ to make the

estimating speed fast and not sensitive to the high frequency noise from the sensors. Gao[17] proposed a method of assigning all the observer eigenvalues at $-\omega_{\mathrm{o}}$ to get the optimal estimating performance by simply tuning a single parameter. Equivalently, the gain vector is

$$\boldsymbol{L} = (\beta_1, \beta_2, \beta_3) = (3\omega_{\mathrm{o}}, 3\omega_{\mathrm{o}}^2, \omega_{\mathrm{o}}^3), \tag{22}$$

where ω_{o} is denoted as the bandwidth of the observer. The observer (21) is known as a linear extended state observer (LESO).

With the LESO, a controller that compensates the generalized disturbance can be designed by the feedback linearization method as

$$u = \frac{-z_3 + u_0}{b_0}, \tag{23}$$

where u_0 is the error feedback variable which is a new input to be determined. Substituting the controller (23) into the system (18), we can get

$$\ddot{y} = (f - z_3) + u_0 = \overline{e}_3 + u_0, \tag{24}$$

where $\overline{e}_3$ is the estimation error in z_3. For an ideal observer, we can ignore the estimation error, and then we obtain a simple linear double-integrator relationship between the output and the new input u_0 as

$$\ddot{y} \approx u_0. \tag{25}$$

Hence, the generalized disturbance is estimated and offset, which is to say that the disturbance and the uncertainties involved in generalized disturbance do not need to be mathematically detailed. To design a tracking controller for this double-integrator relation, we select the new input u_0 as

$$u_0 = k_{\mathrm{p}}(r - z_1) - k_{\mathrm{d}} z_2, \tag{26}$$

where r is the reference input. This form of PD controller makes the closed-loop transfer function pure second-order without a zero, and to place all closed-loop poles at $-\omega_{\mathrm{o}}$ which is denoted as the control bandwidth. Choose the PD parameters as

$$k_{\mathrm{d}} = 2\xi\omega_{\mathrm{c}}, \quad k_{\mathrm{p}} = \omega_{\mathrm{c}}^2, \tag{27}$$

where ξ is the damping ratio for reducing oscillation. Then the objective can make the system output y behave as the reference signal by the manipulative variable u as

$$u = -\frac{k_{\mathrm{p}}}{b_0} z_1 - \frac{k_{\mathrm{d}}}{b_0} z_2 - \frac{1}{b_0} z_3 + \frac{k_{\mathrm{p}}}{b_0} r. \tag{28}$$

3.2 Discussion of the stability

As discussed above, LADRC is a combination of the linear estimator and the linear feedback controller. Thus, the stability can be proved in accordance with the separation principle under some assumptions.

3.2.1 Convergence of the LESO

Let $e_i = x_i - z_i, i = 1, 2, 3$. From Eqs. (18) and (21), the observer error can be expressed as

$$\begin{cases} \dot{e}_1 = e_2 - \beta_1 e_1, \\ \dot{e}_2 = e_3 - \beta_2 e_1, \\ \dot{e}_3 = -\beta_3 e_1 + h. \end{cases} \tag{29}$$

Rewrite Eq. (29) as

$$\dot{\boldsymbol{e}} = \boldsymbol{A}_e \boldsymbol{e} + \boldsymbol{E} h, \tag{30}$$

where

$$\boldsymbol{A}_e = \begin{pmatrix} -\beta_1 & 1 & 0 \\ -\beta_2 & 0 & 1 \\ -\beta_3 & 0 & 0 \end{pmatrix}, \quad \boldsymbol{E} = \begin{pmatrix} 0 \\ 0 \\ 1 \end{pmatrix}. \tag{31}$$

For the chosen observer gain $\boldsymbol{L} = (\beta_1, \beta_2, \beta_3) = (3\omega_{\mathrm{o}}, 3\omega_{\mathrm{o}}^2, \omega_{\mathrm{o}}^3)$, the matrix $\boldsymbol{A}$ is stable. For any h which is bounded, Eq. (30) is bounded, and then the LESO is bounded-input bounded-output (BIBO) stable.

3.2.2 Convergence of the LADRC

Theorem 1 *If $h = \dot{f}$ is bounded, the observer* (21) *and the control strategy for the double integrator* (23) *are stable, and then the combined observer and feedback are stable.*

The closed-loop system presented in Eqs. (19)–(28) can be expressed in the state-space form as

$$\begin{pmatrix} \dot{\boldsymbol{X}} \\ \dot{\boldsymbol{Z}} \end{pmatrix} = \begin{pmatrix} \boldsymbol{A} & -\frac{1}{b_0}\boldsymbol{B}\boldsymbol{K} \\ \boldsymbol{L}\boldsymbol{C} & \boldsymbol{A} - \boldsymbol{L}\boldsymbol{C} + \frac{1}{b_0}\boldsymbol{K} \end{pmatrix} \begin{pmatrix} \boldsymbol{X} \\ \boldsymbol{Z} \end{pmatrix} + \boldsymbol{H} \begin{pmatrix} r \\ h \end{pmatrix}, \tag{32}$$

where the matrices $\boldsymbol{A}, \boldsymbol{B}$, and $\boldsymbol{C}$ are presented in Eq. (20), $\boldsymbol{K} = (k_{\mathrm{p}}, k_{\mathrm{d}}, 1)$, and the matrix $\boldsymbol{H}$ is

$$\boldsymbol{H} = \begin{pmatrix} 0 & k_{\mathrm{p}} & 0 & 0 & 0 & 0 \\ 0 & 0 & 1 & 0 & k_{\mathrm{p}} & 0 \end{pmatrix}^{\mathrm{T}}. \tag{33}$$

The eigenvalue of system (32) is

$$\mathrm{eig} \begin{pmatrix} \boldsymbol{A} & -\frac{1}{b_0}\boldsymbol{B}\boldsymbol{K} \\ \boldsymbol{L}\boldsymbol{C} & \boldsymbol{A} - \boldsymbol{L}\boldsymbol{C} + \frac{1}{b_0}\boldsymbol{B}\boldsymbol{K} \end{pmatrix} = \mathrm{eig} \begin{pmatrix} \boldsymbol{A} - \frac{1}{b_0}\boldsymbol{B}\boldsymbol{K} & -\frac{1}{b_0}\boldsymbol{B}\boldsymbol{K} \\ \boldsymbol{0} & \boldsymbol{A} - \boldsymbol{L}\boldsymbol{C} \end{pmatrix}. \tag{34}$$

It is easy to verify that all the eigenvalues of $\boldsymbol{A} - \frac{1}{b_0}\boldsymbol{B}\boldsymbol{K}$ and $\boldsymbol{A} - \boldsymbol{L}\boldsymbol{C}$ have negative real parts. For any r and h which are bounded, Eq. (34) is bounded. Therefore, the LADRC is BIBO stable.

3.3 MIMO decoupling control

Consider the MIMO system (15) in the following form:

$$\begin{cases} \ddot{\boldsymbol{x}} = \boldsymbol{f}(x, \dot{x}, w, \dot{w}, t) + \boldsymbol{B}_m u, \\ \boldsymbol{y} = \boldsymbol{x}, \end{cases} \tag{35}$$

where $\boldsymbol{x} = (x_1, x_2, \cdots, x_6)^{\mathrm{T}}$, $\boldsymbol{f} = (f_1, f_2, \cdots, f_6)^{\mathrm{T}}$, and $\boldsymbol{u} = (u_1, u_2, \cdots, u_6)^{\mathrm{T}}$. If the control matrix

$$\boldsymbol{B}_m = \begin{pmatrix} b_{11} & \cdots & b_{16} \\ \vdots & & \vdots \\ b_{61} & \cdots & b_{66} \end{pmatrix} = \boldsymbol{J}_{\mathrm{p}}^{-1} \boldsymbol{H}_{\mathrm{p}} \tag{36}$$

is reversible, introducing the virtual control matrix $\boldsymbol{U} = \boldsymbol{B}_m \boldsymbol{u}$, the input/output relationship of the ith channel is

$$\begin{cases} \ddot{x}_i = f_i(x, \dot{x}, \cdots, x_6, \dot{x}_6, t) + U_i, \\ y_i = x_i. \end{cases} \tag{37}$$

Then, the virtual control variable U_i of each channel and the system output y_i are in an SISO relationship, that is, U_i and y_i are completely decoupled. The external disturbance and the coupling between different actuators are canceled together as the generalized disturbance by LADRC. Decoupling control can be realized by embedding six LADRCs in parallel between control the vector $\boldsymbol{U}$ and the output $\boldsymbol{y}$. The actual control vector $\boldsymbol{u}$ can be determined by the virtual control vector $\boldsymbol{U}$ as shown in Fig. 5,

$$\boldsymbol{u} = \boldsymbol{B}_m^{-1}\boldsymbol{U}. \tag{38}$$

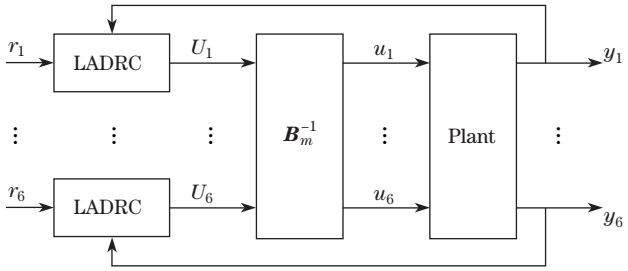

Fig. 5 The diagram of LADRC for an MIMO system

Here, the perturbation of matrix $\boldsymbol{B}_m$ can be rejected in LADRC of each channel, and thus the accurate model of $\boldsymbol{B}_m$ is not necessary to be known. This will be verified in the simulation.

4 Numerical simulation studies

In this section, the model of the 6-DOF vibration isolation system has been developed by using the MATLAB and SIMULINK software to demonstrate the efficiency of the LADRC approach. The parameters for the platform are listed in Table 1. The results of the vibration isolation simulation are presented later.

Table 1 Main parameters of the platform

Parameter	Value
Mass of upper platform	8.14 kg
Moment of inertia of top platform	$\mathrm{diag}(4.1, 4.4, 8) \times 10^{-2}\,\mathrm{kg{\cdot}m^2}$
Moment of inertia of upper leg	$\mathrm{diag}(1.895, 103, 103) \times 10^{-5}\,\mathrm{kg{\cdot}\ m^2}$
Moment of inertia of lower leg	$\mathrm{diag}(9.63, 154, 154) \times 10^{-4}\,\mathrm{kg{\cdot}m^2}$
Mass of each upper leg	0.079 3 kg
Mass of each lower leg	1.16 kg
Stiffness of diaphragm spring	4.8×10^4 N/m

4.1 Frequency response of the system

To investigate the bandwidth of the vibration isolation system, we linearize the open-loop and closed-loop models with the disturbance vector $\boldsymbol{w}$ and output vector $\boldsymbol{y}$ as the system input and output. The open-loop model represents the passive vibration isolation structure, while in contrast, the closed-loop model represents the hybrid vibration isolation system with an active control force. To simplify the diagram, the frequency response of displacement from the base platform to the payload platform along the x-axis is presented. The other input-output combinations respond similarly, with slight differences in resonance frequency and response magnitude.

From the open-loop frequency response shown by the blue curve in Fig. 6, the response of the passive part of the vibration isolation platform has two resonance peaks at 60.6 rad/s and 116.0 rad/s. The open-loop transmission ratio reaches to 24.6 dB. That is to say the passive

structure is a lowpass system which can attenuate the vibration in high frequency band, while the vibration of low frequency passes through the isolation platform completely. The resonance frequencies vary between the different inputs and outputs.

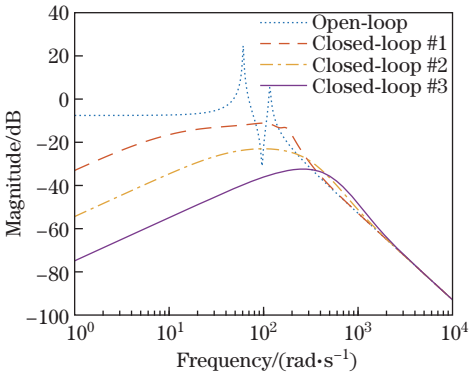

Fig. 6 The frequency response from the base to the payload (color online)

The tuning of control parameters is based on the frequency response of the structure. The two parameters, observer bandwidth ω_o and controller bandwidth ω_c, are gradually increased from the second natural frequency. The closed-loop frequency response is shown in Fig. 6, where the red curve represents the vibration transmission ratio with the parameters $\omega_o = 100$ and $\omega_c = 100$, while the orange and purple curves represent that with the parameters $\omega_o = 500$ and $\omega_c = 100$ and $\omega_o = 500$ and $\omega_c = 500$, respectively. The control signal u for each actuator is limited to $[-50, 50]$ in order to make the system realistic. It is shown that under LADRC, the vibration amplification at frequency lower than 300 rad/s is significantly attenuated, while the vibration amplification at high frequency performs as well as that under passive isolation. At the same time, the resonant peaks of open-loop response disappear in response.

The relation between the parameters and the vibration transmissibility is also clear from Fig. 7. The parameters ω_o and ω_c, which decide the position of closed-loop poles, affect the maneuvering speed and reflect in the bandwidth of the active vibration isolation. The observer bandwidth and the controller bandwidth should cover the bandwidth where the vibration is amplified by the structure.

4.2 Time-domain response

Vibration simulations for the system with the passive vibration isolation structure and active control are respectively tested at fixed frequencies. It is assumed that the displacement and attitude measurements in the inertial frame are obtained by micro-electro-mechanical system (MEMS) sensors and certain multi-sensors fusion algorithm. The initial value of all the states is set to be 0, and the sample rate is set to be 2 000 Hz.

The first case presents the fixed-frequency sinusoidal vibration tests. The displacement amplitude of excitation is given as 10^{-4} m at the resonance frequency of 60.6 rad/s. It can be seen from Fig. 7 that under the parameters $\omega_o = 500$ and $\omega_c = 500$, the system response is attenuated to 1/1 000 of the open-loop response by the active control. The other outputs respond similarly with different attenuating range.

The second case presents the shock test. At time $t = 0.1$ s, we impose a pulse signal with the amplitude of 10^{-3} m and the width of 0.001 s as the shock disturbance. From Fig. 8, the active control can lead to a fast convergence, the time to reach steady state is reduced from 3 s to 0.05 s, and the system response is attenuated to 1/10 of the open-loop response. The other outputs respond in the same trend with different attenuating ranges.

The simulation results of the time response show that the higher controller and observer bandwidth make the output respond faster, which results in better attenuation of the distur-

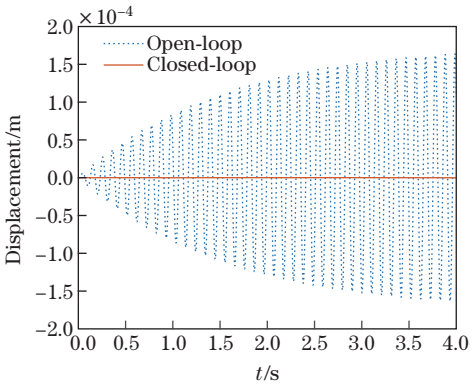

Fig. 7 The response of sinusoidal disturbance (color online)

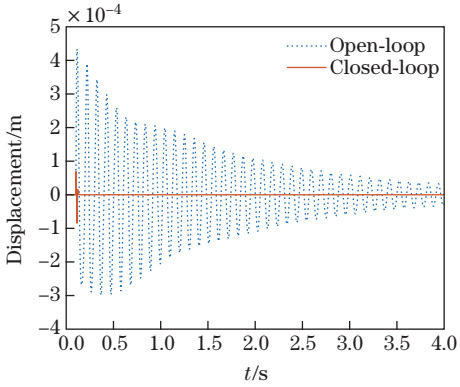

Fig. 8 The response of shock disturbance (color online)

bance and shorter adjustment time when applied in the vibration isolation system. On the other hand, the higher observer bandwidth will make the system more sensitive to the high frequency noise in practical applications. As a conclusion, the optimal control parameters are not obtained by the biggest bandwidth, but should be tuned in a compromise between the vibration attenuation and the noise sensitivity according to the actual working conditions in practical engineering.

4.3 Robustness to the modeling error

Considering the parameters in the control loop, the matrix $\boldsymbol{B}_m^{-1}$ in Eq. (38) is the only variable that contains the information of the controlled plant. To investigate the robustness of the system, we change the structure parameters contained in $\boldsymbol{B}_m$ drastically while keeping the control parameters constant. The frequency response is analyzed with setting the mass and moment of inertia of the payload platform to 0.2 and 5 times of their original values, respectively.

As shown in Fig. 9, the modeling errors in matrix $\boldsymbol{B}_m$ slightly affect the frequency response of the upper platform of the vibration isolation system. The response amplitude of the output becomes only slightly larger as the mass and moment of inertia are estimated 5 times of their actual values. The proposed vibration isolation system performs very robustly to the modeling errors, which can be considered as detailed mathematical model independent.

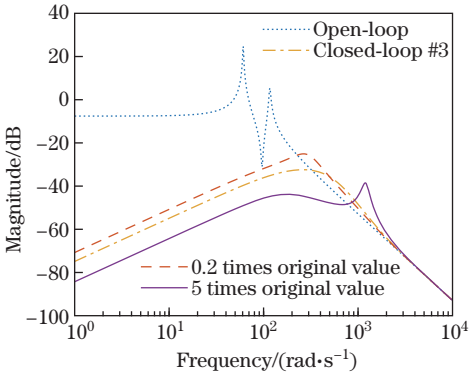

Fig. 9 The frequency response from the base to the payload with modeling error (color online)

5 Conclusions

A practical approach to the 6-DOF vibration isolation system for payloads on spacecrafts by using the LADRC is proposed in this paper. By analyzing the dynamic model of the employed Stewart platform, the order of the control plant is determined. A control solution is then presented based on the LADRC strategy which is independent of the mathematical model, and the system parameters are tuned according to the operating bandwidth. The simulation results show that with the properly tuned LADRC parameters, the vibration isolation system can attenuate the transmission of vibration for about 30 dB in low frequency and eliminate the resonance at the natural frequency effectively, while it performs as well as a passive isolation in high frequency. Furthermore, the robustness of the control system with respect to the modeling error is also verified by drastically changing the parameters of the model.

References

[1] COBB, R. G., SULLIVAN, J. M., DAS, A., DAVIS, L. P., HYDE, T. T., DAVIS, T., RAHMAN, Z. H., and SPANOS, J. T. Vibration isolation and suppression system for precision payloads in space. *Smart Materials and Structures*, **8**(6), 798–812 (1999)

[2] ZHOU, W. Y. and LI, D. X. Design and analysis of an intelligent vibration isolation platform for reaction/momentum wheel assemblies. *Journal of Sound and Vibration*, **331**(13), 2984–3005 (2012)

[3] ZHANG, Y., ZANG, Y., LI, M., WANG, Y. Y., and LI, W. B. Active-passive integrated vibration control for control moment gyros and its application to satellites. *Journal of Sound and Vibration*, **394**, 1–14 (2017)

[4] STEWART, D. A platform with six degrees of freedom. *Proceedings of the Institution of Mechanical Engineers*, **180**(1), 371–386 (1965)

[5] FURQAN, M., SUHAIB, M., and AHMAD, N. Studies on Stewart platform manipulator: a review. *Journal of Mechanical Science and Technology*, **31**(9), 4459–4470 (2017)

[6] FICHTER, E. F. A Stewart platform-based manipulator: general theory and practical construction. *The International Journal of Robotics Research*, **5**(2), 157–182 (1986)

[7] BONEV, I. A. and RYU, J. A new method for solving the direct kinematics of general 6-6 Stewart platforms using three linear extra sensors. *Mechanism and Machine Theory*, **35**(3), 423–436 (2000)

[8] LEBRET, G., LIU, K., and LEWIS, F. L. Dynamic analysis and control of a Stewart platform manipulator. *Journal of Robotic Systems*, **10**(5), 629–655 (1993)

[9] XU, P. and WANG, D. Vibration damping modeling of Stewart platform through Newton-Euler approach. *Proceedings of Smart Structures and Materials* 2005: *Smart Structures and Integrated Systems*, **5764**, 650–661 (2005)

[10] WU, Y., YU, K. P., JIAO, J., CAO, D. Q., CHI, W. C., and TANG, J. Dynamic isotropy design and analysis of a six-DOF active micro-vibration isolation manipulator on satellites. *Robotics and Computer-Integrated Manufacturing*, **49**, 408–425 (2018)

[11] GÁSPÁR, P., SZÁSZI, I., and BOKOR, J. Robust control design for mechanical systems using the mixed μ synthesis. *Periodica Polytechnica Transportation Engineering*, **30**(1-2), 37–52 (2002)

[12] ZHANG, X., SHAO, C., LI, S., XU, D., and ERDMAN, A. G. Robust H_∞ vibration control for flexible linkage mechanism systems with piezoelectric sensors and actuators. *Journal of Sound and Vibration*, **243**(1), 145–155 (2001)

[13] HAN, J. Q. From PID to active disturbance rejection control. *IEEE Transactions on Industrial Electronics*, **56**(3), 900–906 (2009)

[14] ZEINOUN, I. J. and KHORRAMI, F. An adaptive control scheme based on fuzzy logic and its application to smart structures. *Smart Materials and Structures*, **3**(3), 266–276 (1994)

[15] GHABOUSSI, J. and JOGHATAIE, A. Active control of structures using neural networks. *Journal of Engineering Mechanics*, **121**(4), 555–567 (1995)

[16] CURTIS, A. R. An application of genetic algorithms to active vibration control. *Journal of Intelligent Material Systems and Structures*, **2**(4), 472–481 (1991)

[17] GAO, Z. Q. Scaling and bandwidth-parameterization based controller tuning. *Proceedings of Proceedings of the American Control Conference*, **6**, 4989–4996 (2006)